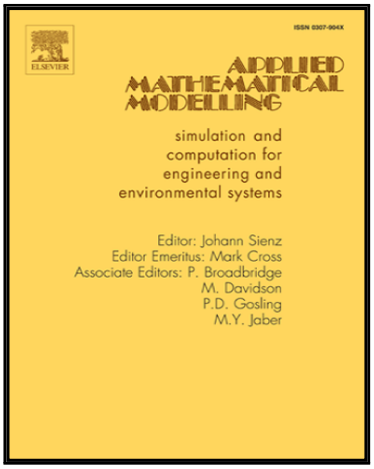

Identification of a multi-dimensional space-dependent heat source from boundary data

M.S. Hussein, D. Lesnic, B.T. Johansson, A. Hazanee

PII: S0307-904X(17)30580-2
DOI: 10.1016/j.apm.2017.09.029
Reference: APM 11974

To appear in: *Applied Mathematical Modelling*

Received date: 18 January 2017
Revised date: 11 September 2017
Accepted date: 13 September 2017

Please cite this article as: M.S. Hussein, D. Lesnic, B.T. Johansson, A. Hazanee, Identification of a multi-dimensional space-dependent heat source from boundary data, *Applied Mathematical Modelling* (2017), doi: 10.1016/j.apm.2017.09.029

Highlights

- Multi-dimensional space-dependent sources are reconstructed from boundary data.
- Iterative regularization methods are developed.
- Convergence and stability of numerical results are thoroughly investigated.

Identification of a multi-dimensional space-dependent heat source from boundary data

M.S. Hussein[1,2], D. Lesnic[2,*], B.T. Johansson[3] and A. Hazanee[4]
[1]*Department of Mathematics, College of Science, University of Baghdad, Baghdad, Iraq*
[2,*]*Department of Applied Mathematics, University of Leeds, Leeds LS2 9JT, UK*
[3]*Mathematics, Aston University EAS, Birmingham, B4 7ET, UK*
[4]*Department of Mathematics and Computer Science, Faculty of Science and Technology, Prince of Songkla University, Pattani Campus, Pattani, 94000, Thailand*
E-mails: mmmsh@leeds.ac.uk, mmmsh@scbaghdad.edu.iq (M.S. Hussein),
amt5ld@maths.leeds.ac.uk (D. Lesnic*-corresponding author),
tomas.johansson@liu.se (B.T. Johansson), areena.h@psu.ac.th (A. Hazanee).

Abstract
We investigate the linear but ill-posed inverse problem of determining a multi-dimensional space-dependent heat source in the parabolic heat equation from Cauchy boundary data. This model is important in practical applications where the distribution of internal sources is to be monitored and controlled with care and accuracy from non-invasive and non-intrusive boundary measurements only. The mathematical formulation ensures that a solution of the inverse problem is unique but the existence and stability are still issues to be dealt with. Even if a solution exists it is not stable with respect to small noise in the measured boundary data hence the inverse problem is still ill-posed. The Landweber method is developed in order to restore stability through iterative regularization. Furthermore, the conjugate gradient method is also developed in order to speed up the convergence. An alternating direction explicit finite-difference method is employed for discretising the well-posed problems resulting from these iterative procedures. Numerical results in two-dimensions are illustrated and discussed.

Keywords: Heat equation; inverse source problem; iterative regularization

1 Introduction

The inverse problem of determining an unknown space-dependent heat source function in the heat equation has been the point of interest of many recent studies, e.g. [1–9]. In these studies, in addition to being mostly restricted to one-dimensional computations, the supplementary information required to compensate for the lack of knowledge of the space-dependent heat source is a final time upper-base, space-dependent internal measurement of the temperature or a time-average of it. However, these measurements are intrusive and may also be difficult to take simultaneously at many space locations at the same fixed specified instant of time. In order to overcome such a situation, one may be able instead to measure non-invasively (the unspecified) boundary data.

The uniqueness of solution of this space-dependent heat source problem was established in related theoretical studies by Cannon [10], Yamamoto [11] and Dinh Nho Hao [12, Subsection 4.3.1]. It is also worth mentioning the extension to two space-dependent additive components heat source identification from Cauchy data investigated theoretically in [13].

The existence of solution is a delicate matter when solving Cauchy problems based on analytic continuation, but anyway, even if the solution does exist it will not depend

continuously on the input data. Thus, the problem is ill-posed and it is the purpose of this study to develop a stable algorithm for solving the inverse space-dependent source problem with Cauchy data and implement this algorithm numerically in two-dimensions.

The plan of the paper is as follows. The two-dimensional inverse space-dependent source problem for the heat equation is formulated in Section 2. The additional boundary measurement is prescribed as an overdetermination condition to ensure the uniqueness of the solution. The Landweber iterative method for solving the linear but ill-posed inverse source problem is described in Section 3. It consists of solving a sequence of direct and adjoint problems until a prescribed stopping criterion is satisfied. In Section 4, an alternating direction explicit finite-difference method is described and numerical results are presented and discussed. In Section 5, the conjugate gradient method is developed in order to speed up the convergence. Section 6 investigates numerically a test example mimicking a point source. Finally, Section 7 presents the conclusions of the paper and possible future work.

2 Mathematical formulation

Let $T > 0$ and Ω be a bounded domain with piecewise sufficiently smooth boundary $\partial\Omega$. Consider the inverse source problem of finding the pair $(u(\mathbf{x},t), f(\mathbf{x}))$ satisfying

$$u_t = \nabla^2 u + r(t)f(\mathbf{x}), \quad (\mathbf{x},t) \in Q_T := \Omega \times (0,T), \tag{1}$$

$$u(\mathbf{x},0) = \phi(\mathbf{x}), \quad \mathbf{x} \in \overline{\Omega}, \tag{2}$$

$$u(\mathbf{x},t) = \beta(\mathbf{x},t) \quad \text{on} \quad \partial\Omega \times (0,T), \tag{3}$$

$$\partial_n u(\mathbf{x},t) = \nu(\mathbf{x},t) \quad \text{on} \quad \Gamma \times (0,T), \tag{4}$$

where $\mathbf{n}$ is the outward unit normal to the boundary $\partial\Omega$, r, ϕ, β and ν are given functions and $\Gamma \subseteq \partial\Omega$ is a subportion of the boundary $\partial\Omega$ on which the measurement of the flux is performed. We can interchange (3) and (4) to specify instead

$$u(\mathbf{x},t) = \beta(\mathbf{x},t) \quad \text{on} \quad \Gamma \times (0,T), \tag{5}$$

$$\partial_n u(\mathbf{x},t) = \nu(\mathbf{x},t) \quad \text{on} \quad \partial\Omega \times (0,T). \tag{6}$$

Obviously, when $\Gamma = \partial\Omega$ then the Cauchy data (3), (4) and (5), (6) coincide, but of practical interest is also to analyse the partial Cauchy data information on the subportion Γ of $\partial\Omega$ as well. We mention that instead of the overspecified data (4) or (5) we can measure the 'upper-base' final temperature

$$u(\mathbf{x},T) = g(\mathbf{x}), \quad \mathbf{x} \in \Omega \tag{7}$$

but this inverse formulation will not be investigated herein; instead we refer to Wang et al. [8] and the references therein.

The uniqueness of a solution $(u(\mathbf{x},t), f(\mathbf{x}))$ of the inverse problem (1)–(4) when $r(t)$ is a constant function (and taken for simplicity to be -1), in which case equation (1) simplifies to

$$u_t = \nabla^2 u - f(\mathbf{x}), \quad (\mathbf{x},t) \in Q_T \tag{8}$$

was established by Cannon [10] using the method of separation of variables. However, when $r(t)$ is not a constant function (or when $r(t)$ is not analytic in time) the proof of uniqueness of a solution is more sophisticated, as provided by Yamamoto [11] for the inverse problem (1), (2), (5) and (6) in the following theorem.

Theorem 1. *Let $\Omega = (0,1)\times(0,1)$, $\Gamma = (0,1)\times\{0\}$ and $r \in C^1[0,T]$ with $r(0) \neq 0$. Let $(f_1(x,y), u_1(x,y,t))$ and $(f_2(x,y), u_2(x,y,t))$ be two solutions of the inverse source problem (1), (2), (5) and (6) which, in terms of the differences $f := f_1 - f_2$ and $u := u_1 - u_2$, satisfy*

$$u_t = \nabla^2 u + r(t) f(x,y), \quad (x,y,t) \in Q_T, \tag{9}$$

$$u(x,y,0) = 0, \quad (x,y) \in \Omega, \tag{10}$$

$$\partial_n u(x,y,t) = 0, \quad (x,y,t) \in \partial\Omega \times (0,T), \tag{11}$$

$$u(x,0,t) = 0, \quad (x,0,t) \in \Gamma \times (0,T). \tag{12}$$

Then, if $f \in L^2(\Omega)$ it follows that $f = 0$ almost everywhere in Ω.

Both Cannon [10] and Yamamoto [11] went on and provided conditional stability estimates for the space-dependent source term in the heat equation in a rectangular domain. However, the admissible sets of sources imposed in those papers are seldom satisfied in practice. Consequently, the inverse problems (1)–(4) or (1), (2), (5), (6) are still ill-posed and small errors in the input data (4) or (5) lead to large errors in the output heat source function $f(\mathbf{x})$. This can easily be realised from the following example, which is a two-dimensional version of the one-dimensional example given in [10].

Example of instability.

Consider the inverse source problem (1)–(4) for $\Omega = (0,1)\times(0,1)$, $T = 1$, $r(t) = -1$, $\Gamma = (0,1)\times\{0\}$, $\beta = \phi = 0$ and

$$-\frac{\partial u}{\partial y}(x,0,t) = \nu(x,0,t) = -\left(\frac{1 - e^{-2m^2\pi^2 t}}{\sqrt{m}\pi}\right)\sin(m\pi x), \quad (x,t) \in (0,1)\times(0,1), \tag{13}$$

where $m \in \mathbb{N}^*$. With this data one can easily check (by direct substitution for example) that the exact solution of the problem (1)–(4) is given by

$$f_m(x,y) = 2\sqrt{m}\sin(m\pi x)\sin(m\pi y), \tag{14}$$

$$u_m(x,y,t) = \left(\frac{1 - e^{-2m^2\pi^2 t}}{m^{3/2}\pi^2}\right)\sin(m\pi x)\sin(m\pi y). \tag{15}$$

It can be seen that, as $m \to \infty$, the input flux data (13) tends to zero, whilst the source function (14) becomes unbounded.

Clearly, in order to restore stability a regularization procedure should be employed and in Section 3 we describe the Landweber method for solving the inverse problems (1)–(4) and (1), (2), (5), (6).

2.1 Direct problem

Consider, for example, the Dirichlet (direct) problem, when f is known, given by equations (1)–(3). This is a well-studied problem that has been shown to have a unique solution in a variety of spaces for different levels of smoothness on the data and domain. For our purpose, we only need well-posedness of (1)–(3) for a class of functions such that the restriction of the normal derivative to the boundary makes sense.

For example, using standard notation, the problem (1)–(3) has a unique solution $u \in L^2(0,T;H^2(\Omega))$, $u_t \in L^2(0,T;L^2(\Omega))$, provided that $r \in C^1[0,T]$, $f \in L^2(\Omega)$, $\beta \in L^2(0,T;H^{3/2}(\partial\Omega)) \cap H^{3/4}(0,T;L^2(\partial\Omega))$, $\phi \in H^1(\Omega)$ with compatibility condition $\beta(\mathbf{x},0) = \phi(\mathbf{x})$ for $\mathbf{x} \in \partial\Omega$. This is shown, for example, in Theorem 9.1, Chapter IV of [14]; note though that an alternative notation is used there with, for example, $W^{2,1}(Q_T)$ meaning $L^2(0,T;H^2(\Omega)) \cap H^1(0,T;L^2(\Omega))$.

For an element $u \in L^2(0,T;H^2(\Omega))$, $u_t \in L^2(0,T;L^2(\Omega))$, by solving the problem (1)–(3) the restriction of the normal derivative of this solution on $\Gamma \times (0,T)$ is well-defined and belongs to $L^2(0,T;H^{1/2}(\Gamma)) \cap H^{1/4}(0,T;L^2(\Gamma))$, see, for example, Lemma 3.4 in Chapter II of [14]. In particular, $\partial_n u|_{\Gamma\times(0,T)} \in L^2(\Gamma \times (0,T))$.

From a practical viewpoint, it might be preferable to only measure function values of the initial state ϕ without having any constraints on the smoothness of derivatives, that is, to have $\phi \in L^2(\Omega)$ rather than $\phi \in H^1(\Omega)$. This can be achieved, for example, by adding some additional smoothness on $r(t)$ and having a homogeneous boundary condition ($\beta = 0$), then the above Dirichlet problem has a unique solution in the above space, with additionally $u \in C^1(0,T;H^2(\Omega))$ for a given $\phi \in L^2(\Omega)$, see Corollary 2.8 in Chapter 7 of [15]. Similar conditions can also be specified for the Neumann (direct) problem, when f is known, given by equations (1), (2) and (6).

For the sake of completeness, we mention that the space $L^2(0,T;X)$, where X is a Hilbert space, consists of measurable functions $u(\cdot,t) : (0,T) \to X$ with $\int_0^T \|u(\cdot,t)\|_X^2 dt < \infty$. By $C^k([0,T];X)$ is understood functions u such that the mapping $u(\cdot,t) : [0,T] \to X$ possesses continuous and bounded (in the usual norm) derivatives of order up to $k \geq 0$. The space $H^k(\Omega)$, $k \geq 0$ is the standard Sobolev space of function having (weak) square integrable derivatives up to order k, with trace space $H^{k-1/2}(\partial\Omega)$.

3 Inverse problem

In the inverse problem, we assume that the space-dependent source component $f(\mathbf{x})$ in the heat equation (1) is unknown.

Throughout this section we assume that $r \in C^1[0,T]$, $r(0) \neq 0$ such that, according to Theorem 1, a solution to the inverse heat source problem (1), (2), (5) and (6) (or (1)–(4)) is unique.

For the Dirichlet inverse problem (1)–(4) we minimize the functional $J_{DN} : L^2(\Omega) \to L^2(\Gamma \times (0,T))$,

$$J_{DN}(f) := \frac{1}{2}\big\|Kf - \nu\big\|^2_{L^2(\Gamma\times(0,T))}, \tag{16}$$

whilst for the Neumann inverse problem (1), (2), (5) and (6) we minimize the functional $J_{ND} : L^2(\Omega) \to L^2(\Gamma \times (0,T))$,

$$J_{ND}(f) := \frac{1}{2}\big\|\tilde{K}f - \beta\big\|^2_{L^2(\Gamma\times(0,T))}, \tag{17}$$

where K and $\tilde{K}$ are operators which will be defined below.

Initially, we have tried to apply the MATLAB toolbox routine *lsqnonlin* for the minimization of the above least-squares functionals but this soon became too much time consuming and hence prohibitive. Thus, the self-coded Landweber iterative algorithm described next was preferred.

Consider first the inverse problem (1)–(4). Introduce the operator $K : L^2(\Omega) \to L^2(\Gamma \times (0,T))$

$$Kf = \partial_n \bar{u}|_{\Gamma\times(0,T)}, \tag{18}$$

where $\bar{u}$ solves the direct well-posed problem

$$\begin{cases} \bar{u}_t = \nabla^2 \bar{u} + r(t)f(\mathbf{x}), \quad (\mathbf{x},t) \in Q_T, \\ \bar{u}(\mathbf{x},0) = 0, \quad \mathbf{x} \in \overline{\Omega}, \\ \bar{u}(\mathbf{x},t) = 0, \quad (\mathbf{x},t) \in \partial\Omega \times (0,T). \end{cases} \tag{19}$$

The operator K is linear and injective (due to the uniqueness of the inverse source problem, [10, 11]). Further, introduce the adjoint problem

$$\begin{cases} v_t = -\nabla^2 v \quad \text{in} \quad Q_T, \\ v(\mathbf{x},T) = 0, \quad \mathbf{x} \in \overline{\Omega}, \\ v(\mathbf{x},t) = 0, \quad (\mathbf{x},t) \in \Gamma^c \times (0,T), \\ v(\mathbf{x},t) = \xi(\mathbf{x},t), \quad (\mathbf{x},t) \in \Gamma \times (0,T), \end{cases} \tag{20}$$

where $\Gamma^c := \partial\Omega \backslash \Gamma$ and ξ is a function to be specified.

Multiplying the first equation in (19) and (20) by v and $\bar{u}$, respectively, and employing Green's formula we obtain (using that $\bar{u}|_{t=0} = v|_{t=T} = 0$, $\bar{u}|_{\partial\Omega\times(0,T)} = 0$, $v|_{\Gamma^c\times(0,T)} = 0$)

$$\begin{aligned} \int_{Q_T} r(t)f(\mathbf{x})v(\mathbf{x},t)\, d\mathbf{x}dt &= \int_{Q_T} (\bar{u}_t - \nabla^2 u)v\, d\mathbf{x}dt + \int_{Q_T} (v_t + \nabla^2 v)\bar{u}\, d\mathbf{x}dt \\ &= -\int_{\Gamma\times(0,T)} v\partial_n \bar{u}\, ds. \end{aligned} \tag{21}$$

Now, using the definition (18) of the operator K together with the specified $v\big|_{\Gamma\times(0,T)} = \xi$, expression (21) can be rewritten as

$$(Kf, \xi)_{L^2(\Gamma\times(0,T))} = (f, K^*\xi)_{L^2(\Omega)}, \tag{22}$$

where the adjoint operator $K^* : L^2(\Gamma \times (0,T)) \to L^2(\Omega)$ is defined by

$$K^*\xi = -\int_0^T r(t)v(\cdot,t)dt, \quad \forall \xi \in L^2(\Gamma \times (0,T)), \tag{23}$$

where v solves the adjoint well-posed problem (20).

Finally, denote by $\tilde{u}$ the solution of the direct problem (1)–(3) with $f = 0$, namely

$$\begin{cases} \tilde{u}_t = \nabla^2 \tilde{u}, \quad \text{in} \quad Q_T, \\ \tilde{u}(\mathbf{x},0) = \phi(\mathbf{x}), \quad \text{in} \quad \overline{\Omega}, \\ \tilde{u}(\mathbf{x},t) = \beta(\mathbf{x},t), \quad (\mathbf{x},t) \in \partial\Omega \times (0,T). \end{cases} \tag{24}$$

One can easily observe that the inverse problem (1)–(4) recasts into solving the linear operational equation

$$Kf = \nu - \partial_n \tilde{u}\big|_{\Gamma\times(0,T)} =: \overline{\nu}. \tag{25}$$

The Landweber method for solving this equation is given by the following iterative procedure:

Step 1. Make an arbitrary initial guess $f_0 \in L^2(\Omega)$ for the source f and solve the direct well-posed problem given by the equations (1) with $f = f_0$, (2) and (3) and denote this solution by u_0.

Step 2. Assume that f_k and u_k have been found. Let v_k solve the well-posed adjoint problem given by the system of equations (20) with

$$\xi(\mathbf{x}, t) := \xi_k(\mathbf{x}, t) = \partial_n u_k(\mathbf{x}, t) - \nu(\mathbf{x}, t), \quad (\mathbf{x}, t) \in \Gamma \times (0, T). \tag{26}$$

Step 3. Put

$$f_{k+1}(\mathbf{x}) = f_k(\mathbf{x}) + \gamma \int_0^T r(t) v_k(\mathbf{x}, t) dt, \quad \mathbf{x} \in \Omega, \tag{27}$$

where $\gamma > 0$ is a relaxation parameter to be prescribed, and let u_{k+1} solve the well-posed direct problem given by equations (1) with $f = f_{k+1}$, (2) and (3).

Step 4. Repeat Steps 2 and 3 until a desired level of accuracy has been achieved (for exact data). For noisy data, use the discrepancy principle to stop the iterations at an appropriate threshold. For more details on the convergence and regularizing character of the Landweber method, see [16].

The inverse problem (1), (2), (5) and (6) is handled similarly by changing the Dirichlet boundary conditions in the direct and adjoint problems (19) and (20) into Neumann boundary conditions. The operator $\tilde{K}$ is then defined as $\tilde{K} f = u|_{\Gamma \times (0,T)}$ and we replace expression (26) by

$$\xi(\mathbf{x}, t) := \xi_k(\mathbf{x}, t) = u_k(\mathbf{x}, t) - \beta(\mathbf{x}, t), \quad (\mathbf{x}, t) \in \Gamma \times (0, T). \tag{28}$$

The adjoint operator is defined as

$$\tilde{K}^* \xi = \int_0^T r(t) v(\mathbf{x}, t) dt, \tag{29}$$

and the plus sign in (27) is changed to minus.

4 Numerical discretisation

The one-dimensional case has been discussed in detail elsewhere, [17, 18], and therefore it will not be considered herein. The two-dimensional case when Ω is a bounded planar domain reflects more the typical properties of the general inverse and ill-posed source problem. For the simplicity of explanation, in the remaining part of the paper we assume that Ω is rectangle and, in fact, we take Ω to be the unit square $(0, 1) \times (0, 1)$, [10, 11]. Then, to discretise equation (1) in the unit square domain $\Omega = (0, 1) \times (0, 1)$,

$$u_t = u_{xx} + u_{yy} + r(t) f(x, y, t), \ (x, y, t) \in Q_T = \Omega \times (0, T) = (0, 1) \times (0, 1) \times (0, T), \tag{30}$$

we subdivide Q_T into M_x, M_y and N subintervals of equal step lengths $\Delta x = 1/M_x$ and $\Delta y = 1/M_y$, and uniform time step $\Delta t = T/N$. At the grid nodes (x_i, y_j, t_k) given by $x_i = i\Delta x$, $y_j = j\Delta y$ and $t_k = k\Delta t$, we denote $u^k_{i,j} := u(x_i, y_j, t_k)$, $r_k := r(t_k)$ and $f_{i,j} := f(x_i, y_j)$ for $i = \overline{0, M_x}$, $j = \overline{0, M_y}$ and $k = \overline{0, N}$.

4.1 Alternating direction explicit method (ADEM)

Based on the method described in [19], in this section an unconditionally stable numerical procedure for solving the heat equation (30) with initial and boundary conditions (2) and (3) will be outlined.

Let $\tilde{u}_{i,j}^k$ and $\tilde{v}_{i,j}^k$ be the solutions of the following equations which are multilevel finite-difference discretisations of (30):

$$\frac{\tilde{u}_{i,j}^{k+1}-\tilde{u}_{i,j}^k}{\Delta t}=\frac{\tilde{u}_{i+1,j}^k-\tilde{u}_{i,j}^k-\tilde{u}_{i,j+1}^{k+1}+\tilde{u}_{i-1,j}^{k+1}}{(\Delta x)^2}+\frac{\tilde{u}_{i,j+1}^k-\tilde{u}_{i,j}^k-\tilde{u}_{i,j}^{k+1}+\tilde{u}_{i,j-1}^{k+1}}{(\Delta y)^2}+r_k f_{i,j},$$
$$i=\overline{1,M_x-1},\quad j=\overline{1,M_y-1},\quad k=\overline{0,N}, \tag{31}$$

$$\frac{\tilde{v}_{i,j}^{k+1}-\tilde{v}_{i,j}^k}{\Delta t}=\frac{\tilde{v}_{i+1,j}^{k+1}-\tilde{v}_{i,j}^{k+1}-\tilde{v}_{i,j}^k+\tilde{v}_{i-1,j}^k}{(\Delta x)^2}+\frac{\tilde{v}_{i,j+1}^{k+1}-\tilde{v}_{i,j}^{k+1}-\tilde{v}_{i,j}^k+\tilde{v}_{i,j-1}^k}{(\Delta y)^2}+r_k f_{i,j},$$
$$i=\overline{M_x-1,1},\quad j=\overline{M_y-1,1},\quad k=\overline{0,N}. \tag{32}$$

We approximate $u_{i,j}^{k+1}$ as the arithmetic mean of $\tilde{u}_{i,j}^{k+1}$ and $\tilde{v}_{i,j}^{k+1}$, namely,

$$u_{i,j}^{k+1}=\frac{\tilde{u}_{i,j}^{k+1}+\tilde{v}_{i,j}^{k+1}}{2}. \tag{33}$$

Rearranging the terms in (31) and (32), we obtain the explicit calculations of $\tilde{u}_{i,j}^k$ and $\tilde{v}_{i,j}^k$:

$$\tilde{u}_{i,j}^{k+1}=a\tilde{u}_{i,j}^k+b(\tilde{u}_{i-1,j}^{k+1}+\tilde{u}_{i+1,j}^k)+c(\tilde{u}_{i,j-1}^{k+1}+\tilde{u}_{i,j+1}^k)$$
$$+\frac{\Delta t}{1+\lambda}r_k f_{i,j},\quad i=\overline{1,M_x-1},\quad j=\overline{1,M_y-1},\quad k=\overline{0,N}, \tag{34}$$

$$\tilde{v}_{i,j}^{k+1}=a\tilde{v}_{i,j}^k+b(\tilde{v}_{i-1,j}^k+\tilde{v}_{i+1,j}^{k+1})+c(\tilde{v}_{i,j-1}^k+\tilde{v}_{i,j+1}^{k+1})$$
$$+\frac{\Delta t}{1+\lambda}r_k f_{i,j},\quad i=\overline{M_x-1,1},\quad j=\overline{M_y-1,1},\quad k=\overline{0,N}. \tag{35}$$

where

$$a=\left[1-\Delta t\left(\frac{1}{(\Delta x)^2}+\frac{1}{(\Delta y)^2}\right)\right]\Big/\left[1+\Delta t\left(\frac{1}{(\Delta x)^2}+\frac{1}{(\Delta y)^2}\right)\right]=\frac{1-\lambda}{1+\lambda},$$
$$b=\frac{\Delta t}{(\Delta x)^2}/(1+\lambda),\quad c=\frac{\Delta t}{(\Delta y)^2}/(1+\lambda),\quad \lambda=\Delta t\left(\frac{1}{(\Delta x)^2}+\frac{1}{(\Delta y)^2}\right).$$

The initial and boundary conditions (2) and (3) in discretised form are

$$u_{i,j}^0=\phi_{i,j},\quad i=\overline{0,M_x},\quad j=\overline{0,M_y}, \tag{36}$$

$$u_{0,j}^k=\beta_{0,j}^k,\ u_{M_x,j}^k=\beta_{M_x,j}^k,\ j=\overline{0,M_y},\ u_{i,0}^k=\beta_{i,0}^k,\ u_{i,M_y}^k=\beta_{i,M_y}^k,\ i=\overline{0,M_x},\ k=\overline{1,N}, \tag{37}$$

where $\phi_{i,j}=\phi(x_i,y_j)$, $\beta_{0,j}^k=\beta(0,y_j,t_k)$, $\beta_{M_x,j}^k=\beta(1,y_j,t_k)$, $\beta_{i,0}^k=\beta(x_j,0,t_k)$ and $\beta_{i,M_y}^k=\beta(x_j,1,t_k)$ for $i=\overline{0,M_x}$, $j=\overline{0,M_y}$, $k=\overline{1,N}$.

From (34), $\tilde{u}_{i,j}^{k+1}$ can be computed explicitly. In this case, calculations proceed from the grid point close to the boundaries $x=0$ and $y=0$, as i, j increase. The needed values such as $\tilde{u}_{i-1,j}^{k+1}$, $\tilde{u}_{i,j}^k$ and $\tilde{u}_{i+1,j}^k$ will be known from the initial and boundary conditions (36) and (37). Similarly, $\tilde{v}_{i,j}^{k+1}$ can be calculated explicitly from (35) beginning at the boundaries $x=1$ and $y=1$ and then marching in a sequence of decreasing i and j, i.e.

$i = M_x - 1, M_x - 2, \cdots, 1$, $j = M_y - 1, M_y - 2, \cdots, 1$. These values are substituted into (33) to obtain the solution $u_{i,j}^{k+1}$.

This procedure is unconditionally stable, as both equations (34) and (35) are unconditionally stable, but the time increment Δt cannot be taken indefinitely large. It has been noticed in [19] that if the time increment is taken very large, the solution obtained will be stable but may not describe the actual and physical problem. This behavior is common to all unconditionally stable explicit or semi-implicit methods.

When the Neumann flux boundary condition (6) is given instead of the Dirichlet boundary condition (3), then we approximate it as

$$\begin{cases} \nu_{0,j}^k = \dfrac{4u_{1,j}^k - u_{2,j}^k - 3u_{0,j}^k}{2\Delta x}, \quad j = \overline{1, M_y - 1}, \quad k = \overline{1, N}, \\ \nu_{M_x,j}^k = \dfrac{4u_{M_x-1,j}^k - u_{M_x-2,j}^k - 3u_{M_x,j}^k}{-2\Delta x}, \quad j = \overline{1, M_y - 1}, \quad k = \overline{1, N}, \\ \nu_{i,0}^k = \dfrac{4u_{i,1}^k - u_{i,2}^k - 3u_{i,0}^k}{2\Delta y}, \quad i = \overline{1, M_x - 1}, \quad k = \overline{1, N}, \\ \nu_{i,M_y}^k = \dfrac{4u_{i,M_y-1}^k - u_{i,M_y-2}^k - 3u_{i,M_y}^k}{-2\Delta y}, \quad i = \overline{1, M_x - 1}, \quad k = \overline{1, N}. \end{cases} \tag{38}$$

4.2 Numerical solution of the inverse problem

We aim to obtain stable reconstructions for the heat source $f(x, y)$ together with the temperature $u(x, y, t)$ satisfying the equations (2)–(4) and (30) for the Dirichlet problem or, equations (2), (5), (6) and (30) for the Neumann problem. To assess the accuracy of the numerical solution for the heat source we define the root mean square error by:

$$rmse(f) = \left[\frac{1}{(M_x - 1)(M_y - 1)} \sum_{i=1}^{M_x - 1} \sum_{j=1}^{M_y - 1} \left(f^{numerical}(x_i, y_j) - f^{exact}(x_i, y_j) \right)^2 \right]^{1/2}. \tag{39}$$

The space grid meshing of the unit square $\Omega = (0, 1) \times (0, 1)$ is kept fixed at $M_x = M_y = 10$ throughout the computations. The integral involved in (27) is simply approximated by the point rule

$$\int_0^T r(t) v_k(x, y, t) dt \approx \frac{T}{N} \sum_{i=0}^{N-1} r(t_i) v_k(x, y, t_i), \quad (x, y) \in \Omega. \tag{40}$$

We consider solving the Dirichlet inverse problem (2)–(4) and (30) with the input data given by

$$r(t) = 1, \quad t \in (0, T), \tag{41a}$$
$$\phi(x, y) = 0, \quad (x, y) \in (0, 1) \times (0, 1), \tag{41b}$$
$$\beta(x, y, t) = 0, \quad (x, y, t) \in \partial\Omega \times (0, T), \tag{41c}$$

and the heat flux measurement

$$\partial_n u(0, y, t) = \nu(0, y, t) = -\pi(e^{-2t\pi^2} - 1) \sin(\pi y), \quad (y, t) \in (0, 1) \times (0, T), \tag{42}$$

for $\Gamma = \{0\} \times (0,1)$ and $T = 1$. The analytical solution of this problem is given by

$$u(x,y,t) = \big(\exp(-2\pi^2 t) - 1\big)\sin(\pi x)\sin(\pi y), \quad (x,y,t) \in (0,1)\times(0,1)\times(0,T), \tag{43}$$

and

$$f(x,y) = -2\pi^2 \sin(\pi x)\sin(\pi y), \quad (x,y) \in (0,1)\times(0,1). \tag{44}$$

As we also need to illustrate the convergence of the least-squares objective function (16), this is numerically discretised, as

$$J_{DN}(f) = \frac{1}{2}\|Kf - \nu\|^2_{L^2(\Gamma\times(0,T))} \approx \frac{T}{2N(M_y-1)} \sum_{j=1}^{M_y-1}\sum_{i=1}^{N} (\nu^i_{0,j} - \nu(0,y_j,t_i))^2. \tag{45}$$

We take the initial guess $f^0 = 0$ for the heat source.

For exact data, i.e. no noise in the heat flux measurement (42), we illustrate in Figure 1 the convergence of the objective function (16), as a function of the number of iterations, for various time grids $N \in \{50, 100, 200\}$ and various relaxation parameters $\gamma \in \{1, 5, 10\}$ in (27). For values of γ greater than about 11 the objective function (16) was found to diverge. This is expected since it is well-known that there exists an upper bound condition $\gamma < \|K\|^{-2}$ under which convergence of the Landweber method is assured, [16]. From Figure 1 it can be seen that, after about 200 iterations, the objective function significantly decreases as N increases. Also, the rate of convergence increases with increasing γ. The corresponding absolute errors between the numerically retrieved heat source and the exact solution (44) illustrated in Figures 3–5, as well as the $rmse(f)$ values calculated from (39) and given in Figure 2 and Table 1 all confirm the convergence and excellent performance of the iterative Landweber method with ADE for solving the inverse Dirichlet heat source problem for exact data. As shown in Figure 2, the FDM mesh with $N = 50$ is too coarse and the semi-convergence phenomenon, [16], of the iterative regularization clearly manifests.

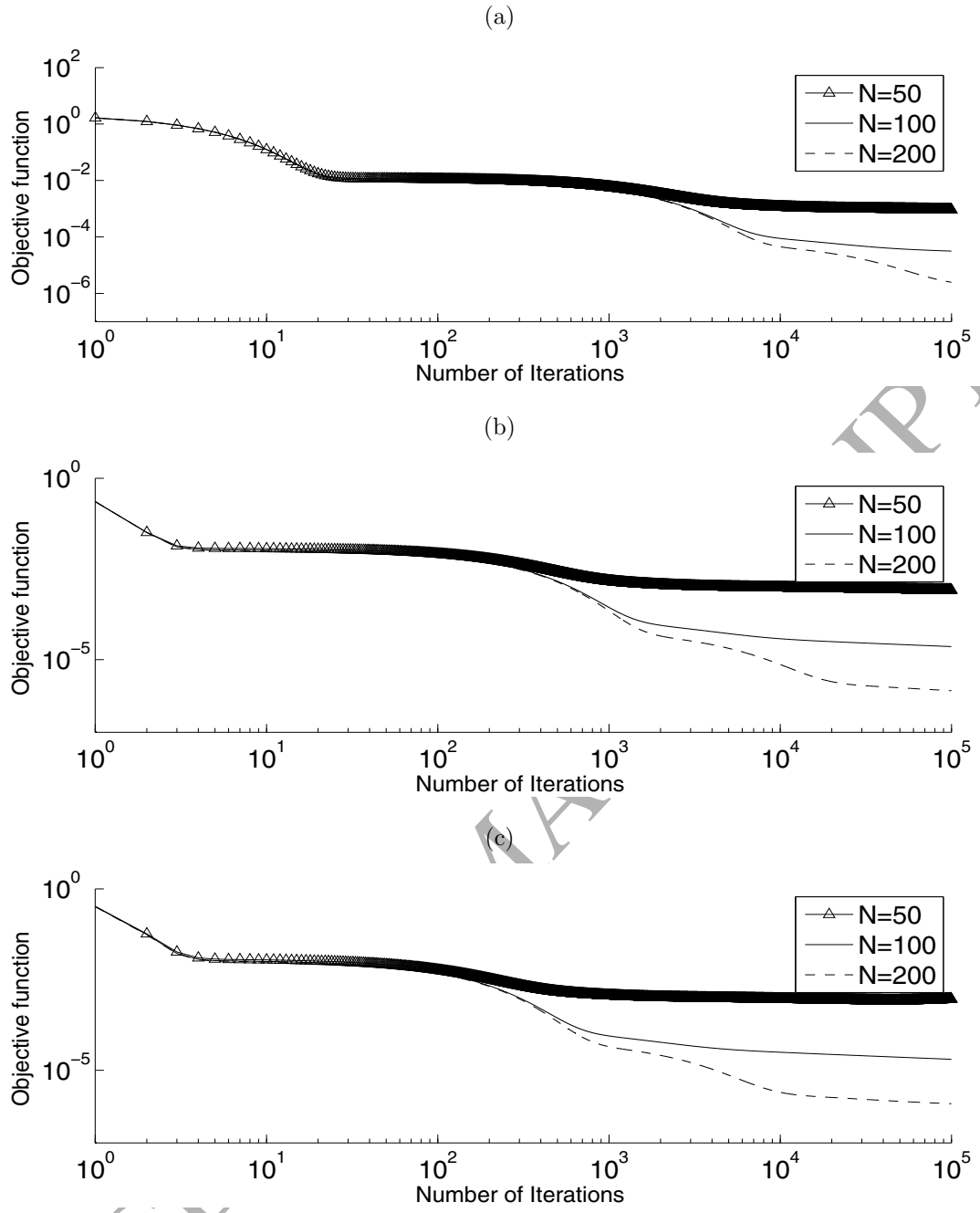

Figure 1: The objective function J_{DN} in (16), as a function of the number of iterations, for $N \in \{50, 100, 200\}$ and (a) $\gamma = 1$, (b) $\gamma = 5$, (c) $\gamma = 10$.

(a)

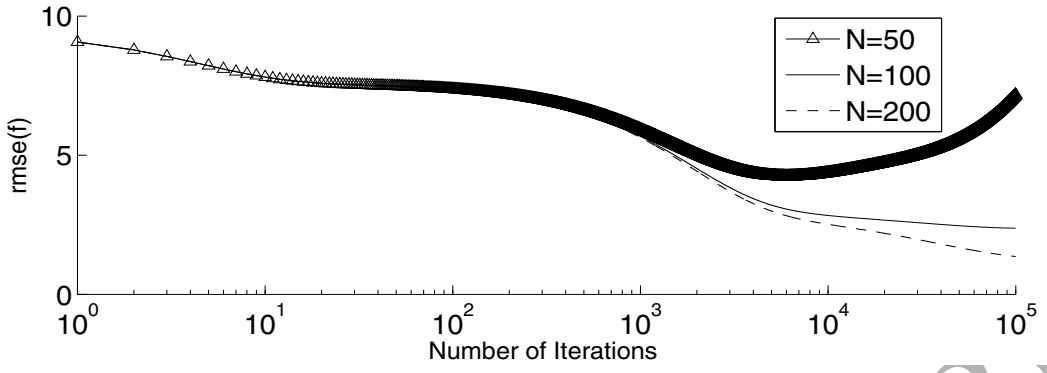

(b)

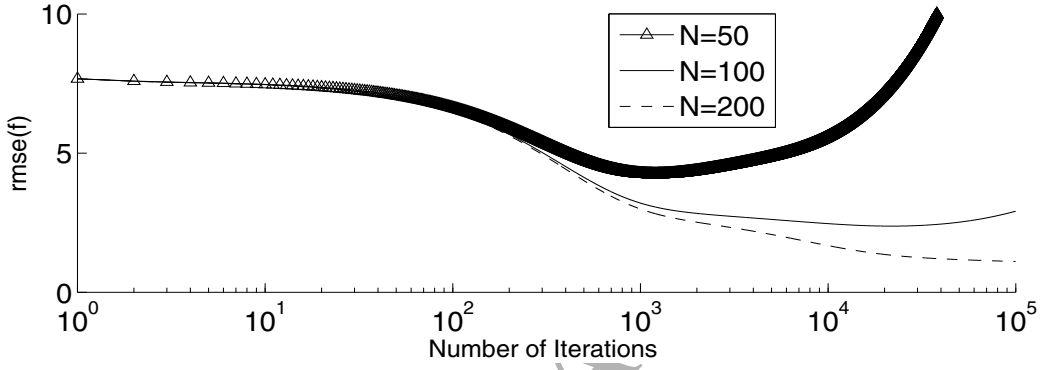

(c)

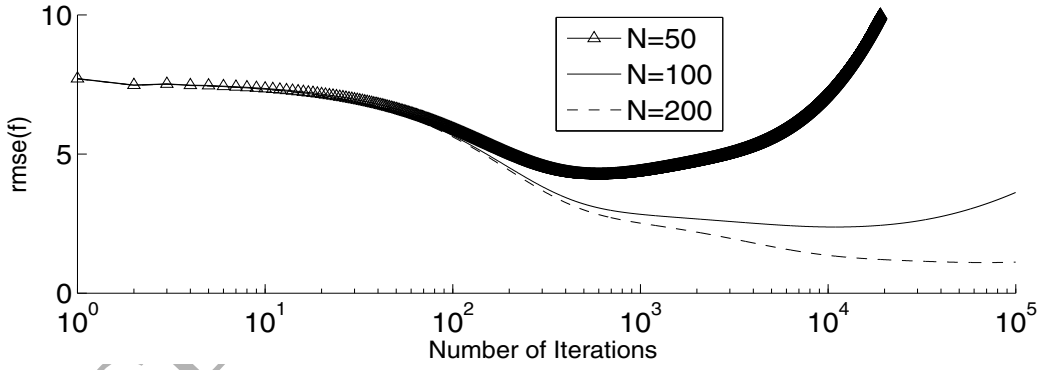

Figure 2: The $rmse(f)$ in (39), as a function of the number of iterations, for $N \in \{50, 100, 200\}$ and (a) $\gamma = 1$, (b) $\gamma = 5$, (c) $\gamma = 10$.

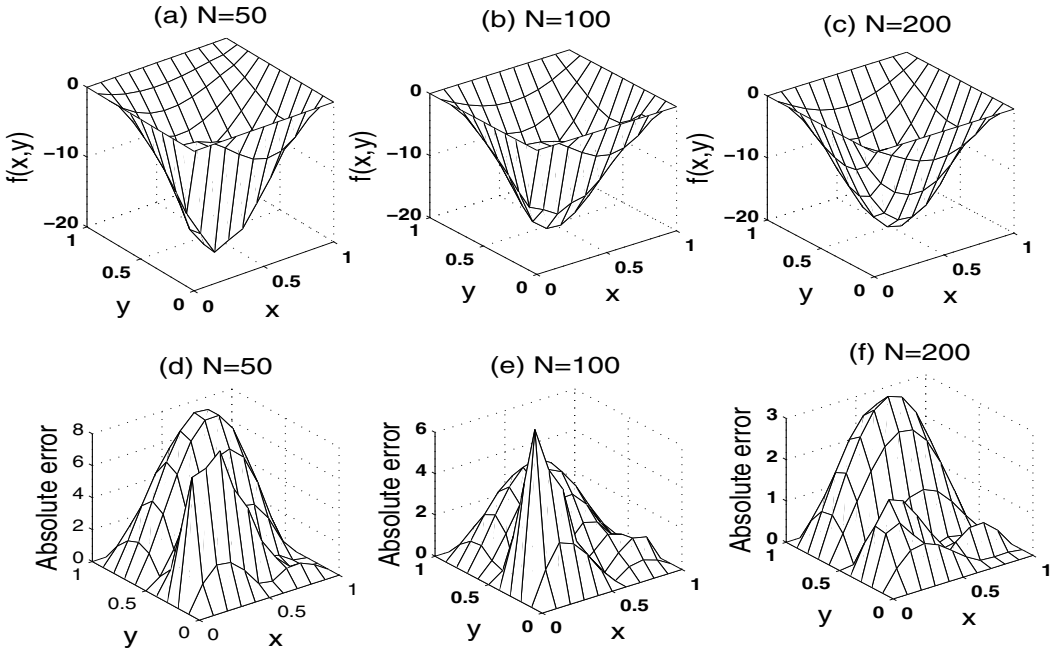

Figure 3: The numerical solutions and the absolute error between the numerical and the exact solutions, for the heat source with $\gamma = 1$, and $N = 50$, plotted at iteration 6087 which is the minimum point of $rmse(f)$ in Figure 2(a), $N = 100$ and $N = 200$.

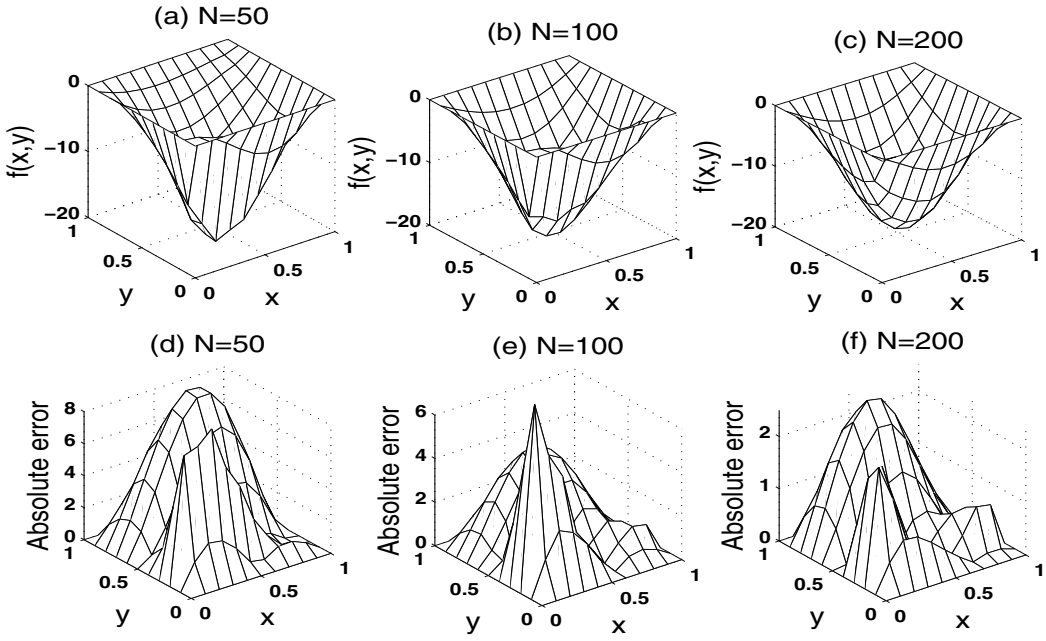

Figure 4: The numerical solutions and the absolute error between the numerical and exact solutions for the heat source with $\gamma = 5$, and $N = 50$, plotted at iteration 1216 which is the minimum point of $rmse(f)$ in Figure 2(b), $N = 100$, plotted at iteration 21925 which is the minimum point of $rmse(f)$ in Figure 2(b), and $N = 200$.

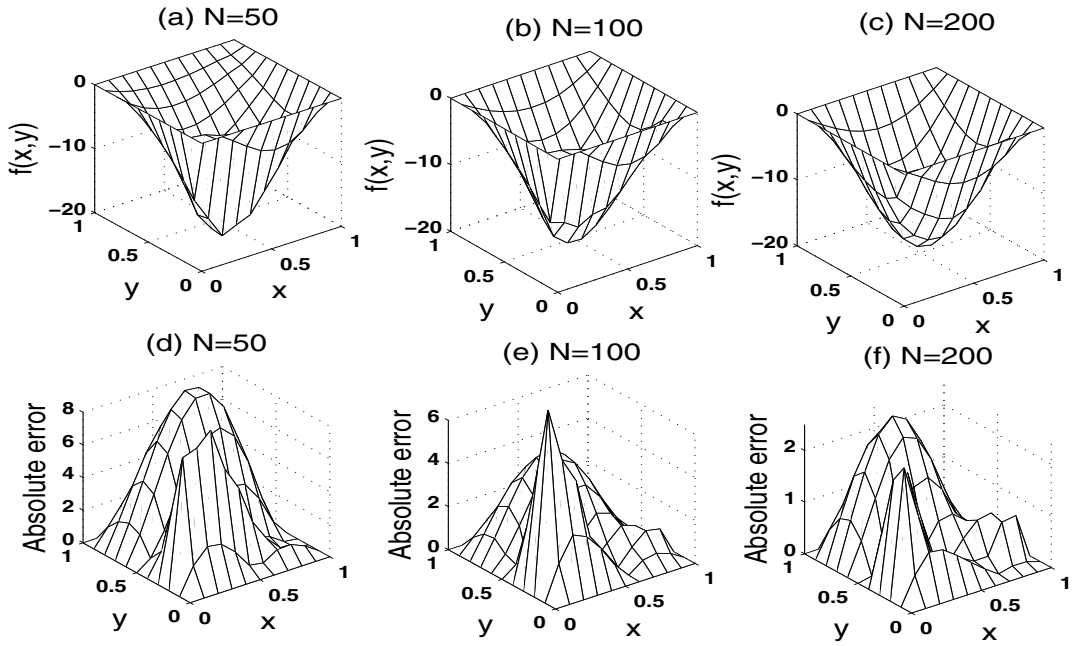

Figure 5: The numerical solutions and the absolute error between the numerical and exact solutions, for the heat source with $\gamma = 10$, and $N = 50$, plotted at iteration 605 which is the minimum point of $rmse(f)$ in Figure 2(c), $N = 100$, plotted at iteration 10976 which is the minimum point of $rmse(f)$ in Figure 2(c), and $N = 200$, plotted at iteration 69664 which is the minimum point of $rmse(f)$ in Figure 2(c).

Table 1: The minimum values of $rmse(f)$ for $N \in \{50, 100, 200, 400\}$ and $\gamma \in \{1, 5, 10\}$.

N \ γ	1	5	10
50	4.7104	4.7102	4.7099
100	2.6418	2.6403	2.6403
200	1.5091	1.2313	1.2209
400	2.4603	1.5003	1.1313

The computational times to run 10^5 iterations on a laptop machine, with Intel core i7 at 2.2 GHz processor and 8 GB of memory are approximately 13, 24 and 42 hours for $N \in \{50, 100, 200\}$, respectively. This may imply some slow convergence and high computational time but then the speeding up can be achieved either by increasing γ or by using a variable γ (depending on the iterative number k) in (27), as in the conjugate gradient method, [5, 16], described in the next section.

Next we fix $N = 100$, $\gamma = 10$ and consider the case of noisy data (4). This is numerically simulated by perturbing the heat flux measurement (42) with Gaussian additive random noise ϵ with mean zero and standard deviation

$$\sigma = p \times \max_{(y,t)\in(0,1)\times(0,T)} |\nu(0, y, t)|, \tag{46}$$

where p represents the percentage of noise, as follows:

$$\nu^{\epsilon}(0, y_j, t_i) = \nu(0, y_j, t_i) + \epsilon_{j,i}, \quad j = \overline{1, M_y - 1}, i = \overline{1, N}. \tag{47}$$

We use the MATLAB function *normrnd* to generate the random variables $\underline{\epsilon} = (\epsilon_{j,i})_{i=\overline{1,N}, j=\overline{1,M_y-1}}$, as follows:

$$\underline{\epsilon} = normrnd(0, \sigma, M_y - 1, N). \tag{48}$$

In the case of noisy data (47), we replace $\nu(0, y_j, t_i)$ by $\nu^{\epsilon}(0, y_j, t_i)$ in (16). The total amount of noise

$$\varepsilon(p) := \|\nu^{\epsilon} - \nu^{exact}\| = \sqrt{\frac{T}{N(M_y - 1)} \sum_{j=1}^{M_y-1} \sum_{i=1}^{N} (\nu^{noise}(0, y_j, t_i) - \nu(0, y_j, t_i))^2}, \tag{49}$$

generated from one of these simulations is $\varepsilon(p) \in \{0.1374, 0.2749\}$ for $p \in \{5, 10\}\%$, respectively. This is important to know because in order to obtain a stable solution we need to stop the iterative process described in Section 3 at the first iteration number k_d for which the discrepancy criterion

$$J_{DN}(f_{k_d}) \leq \tau \frac{\varepsilon^2(p)}{2}, \tag{50}$$

where τ is some constant greater than unity, is satisfied, [6, 16].

Figures 6(a) and 6(b) show the objective function (16) and the $rmse(f)$, respectively, for the first 10^5 iterations for various percentages of noise $p \in \{5, 10\}\%$, for $\tau = 1.3$. This yields the thresholds in (50) given by $\tau \frac{\varepsilon^2(p)}{2} \in \{0.0123, 0.0491\}$ for $p \in \{5, 10\}\%$, respectively.

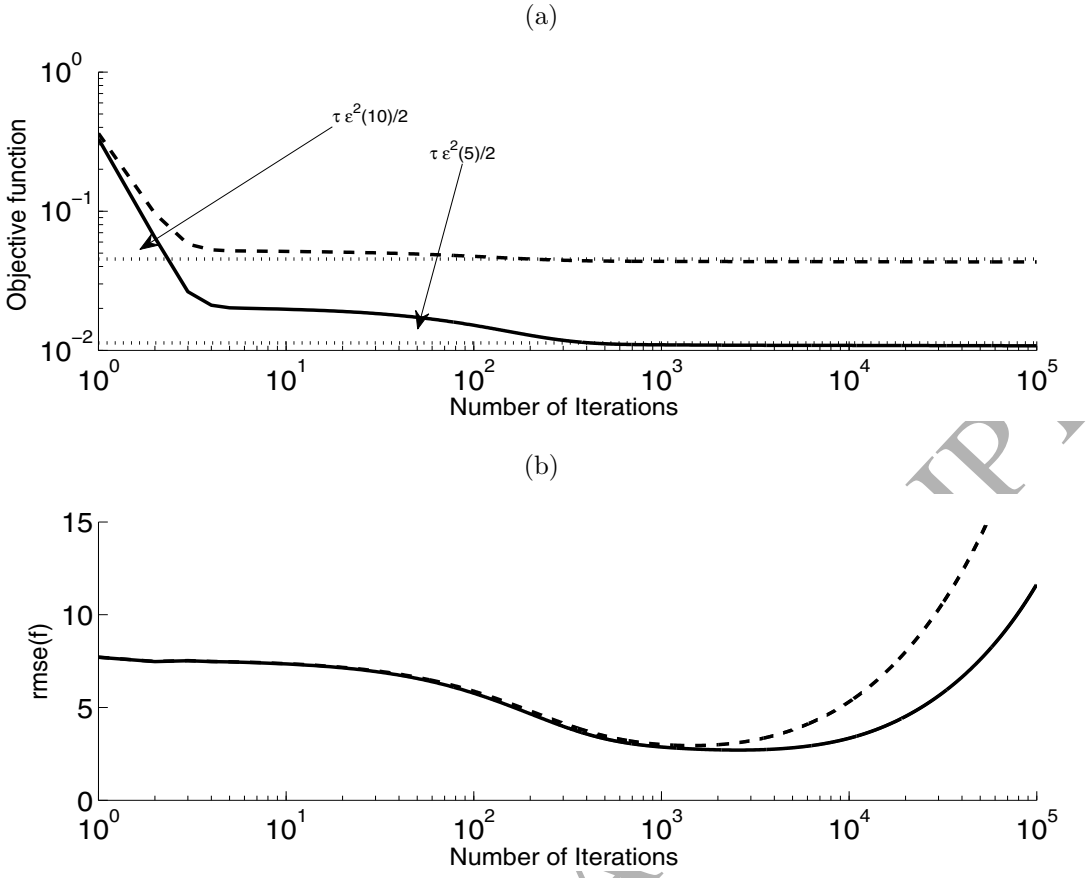

Figure 6: (a) The objective function (16) and (b) the $rmse(f)$, as functions of the number of iterations, for various noise levels $p = 5\%(\text{——})$ and $p = 10\%(- - -)$.

According to the discrepancy principle criterion (50), we terminate the iterations of the algorithm at the iteration number k_d

$$k_d = \begin{cases} 560, & \text{for } p = 5\%, \\ 306, & \text{for } p = 10\%, \end{cases} \qquad rmse(f_{k_d}) = \begin{cases} 3.5659, & \text{for } p = 5\%, \\ 4.5854, & \text{for } p = 10\%. \end{cases} \tag{51}$$

As expected, as p increases from 5% to 10% the iterations should be stopped earlier. From Figure 6(b) it can be seen that the objective function (16) decreases as the number of iterations k increases but the $rmse(f)$ starts increasing once

$$k > k_{opt} = \begin{cases} 2618, & \text{for } p = 5\%, \\ 1467, & \text{for } p = 10\%, \end{cases} \qquad rmse(f_{k_{opt}}) = \begin{cases} 3.0053, & \text{for } p = 5\%, \\ 3.2750, & \text{for } p = 10\%. \end{cases} \tag{52}$$

Figures 7(a,b) and 7(c,d) illustrate the absolute errors between the exact solution (44) and the numerically retrieved heat source at the iterations k_d and k_{opt} given by (51) and (52), respectively, for $p \in \{5, 10\}\%$ noise. From these figures and equations (51) and (52) it can be seen that the accuracy of the numerical solutions improves as the amount of noise decreases from $p = 10\%$ to 5%. Moreover, by comparing Figures 7(a,b) and 7(c,d) it can be seen that although the numerical source solution $f(k_{opt})$ is more accurate than $f(k_d)$ it is less stable. This is expected since the Landweber method is a regularizing semi-convergent iterative algorithm which should be stopped according to the discrepancy

principle (50). Moreover, in practice only k_d can be computed as k_{opt} uses the knowledge of the analytical solution which is not available in general.

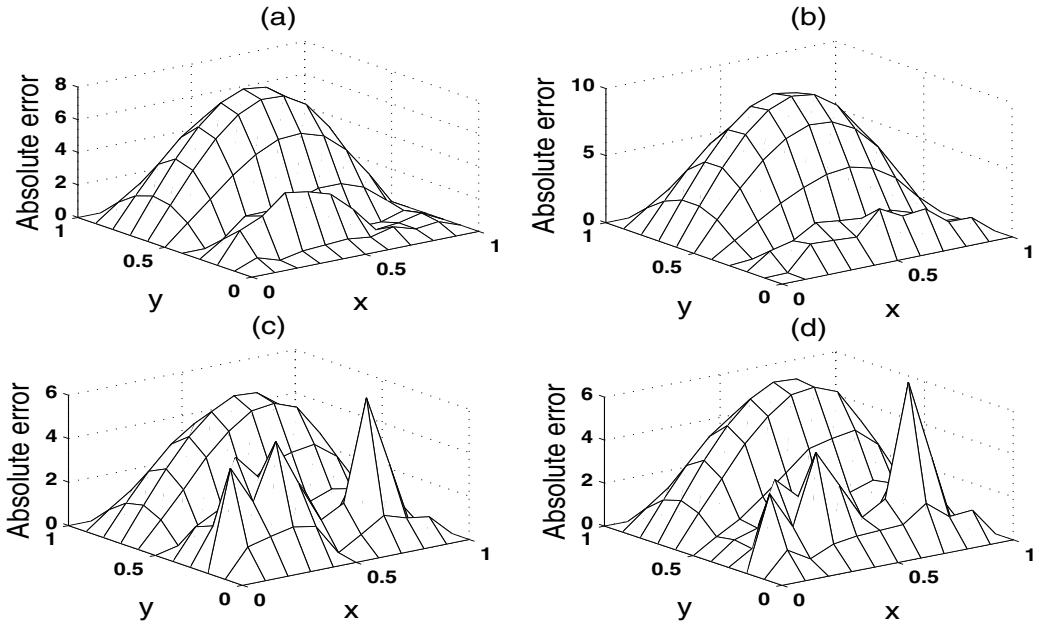

Figure 7: The absolute error between the exact (44) and numerical solutions $f(k_d)$ for (a) $p = 5\%$ and (b) $p = 10\%$ noise. The absolute error between the exact (44) and numerical solutions $f(k_{opt})$ for (c) $p = 5\%$ and (d) $p = 10\%$ noise.

5 The conjugate gradient method

From the previous numerical investigation it was observed that the convergence of the Landweber iterative method described in Section 3 can become prohibitively slow even when the relaxation parameter γ in (27) increases. For example, as previously reported it takes 1 day to run 10^5 iterations for $M_x = M_y = 10$ and $N = 100$, $\gamma = 10$ to achieve the $rmse(f) = 2.6403$. In order to speed up the convergence of minimization of the least-squares functional (16) (or (17)) we can improve on the Landweber method and employ instead the regularising γ-free conjugate gradient method (CGM). This iterative algorithm runs as follows.

Let Steps 1 and 2 be the same as in the Landweber algorithm of Section 3. The next steps are as follows:

Step 3 Calculate

$$d_k(\mathbf{x}) = -z_k(\mathbf{x}) + \beta_{k-1} d_{k-1}(\mathbf{x}), \qquad k \geq 0 \tag{53}$$

with the convention that $\beta_{-1} = 0$ and

$$\beta_{k-1} = \frac{\|z_k\|^2_{L^2(\Omega)}}{\|z_{k-1}\|^2_{L^2(\Omega)}}, \qquad k \geq 1, \tag{54}$$

where the gradient (23) is given by

$$z_k(\mathbf{x}) = -\int_0^T r(t) v_k(\mathbf{x}, t) dt, \qquad k \geq 0. \tag{55}$$

Step 4 Solve the direct well-posed problem given by the equations (19) with $f = d_k$, to determine Kd_k defined by (18). Set

$$\alpha_k = \frac{\|z_k\|^2_{L^2(\Omega)}}{\|Kd_k\|^2_{L^2(\Gamma\times(0,T))}}, \qquad k \geq 0, \tag{56}$$

and pass to the new iteration by letting

$$f_{k+1}(\mathbf{x}) = f_k(\mathbf{x}) + \alpha_k d_k(\mathbf{x}), \qquad k \geq 0. \tag{57}$$

Step 5 This step is the same as Step 4 of the Landweber algorithm of Section 3.

In what follows, we consider the same example as in Section 4. We take $M_x = M_y = 10$. The $L^2(\Omega)$-norm of the functions involved in (54) and (56) is calculated as

$$\|z\|^2_{L^2(\Omega)} = \frac{1}{(M_x-1)(M_y-1)} \sum_{i=1}^{M_x-1} \sum_{j=1}^{M_y-1} z^2(x_i, y_j). \tag{58}$$

For exact data, Figures 8(a) and 8(b) show the objective function J_{DN} in (16) and the $rmse(f)$ in (39), respectively, as functions of the number of iterations, for various $N \in \{50, 100, 200\}$. The corresponding absolute errors between the exact solution (44) and the numerical CGM heat source are shown in Figure 9.

The minimum values for $rmse(f)$ are $rmse(f) \in \{4.5997, 2.5783, 1.5583, 1.1328\}$ for $N \in \{50, 100, 200, 400\}$, respectively. By comparing these values to those obtained in Table 1 obtained with the Landweber method (compare also Figure 8(a) with Figure 1, Figure 8(b) with Figure 2, and Figure 9 with Figures 3–5) it can be seen that the CGM gains at least two orders of magnitude speed of convergence, i.e. the CGM uses 10^3 iterations instead of 10^5 required by the Landweber method to achieve the same level of accuracy.

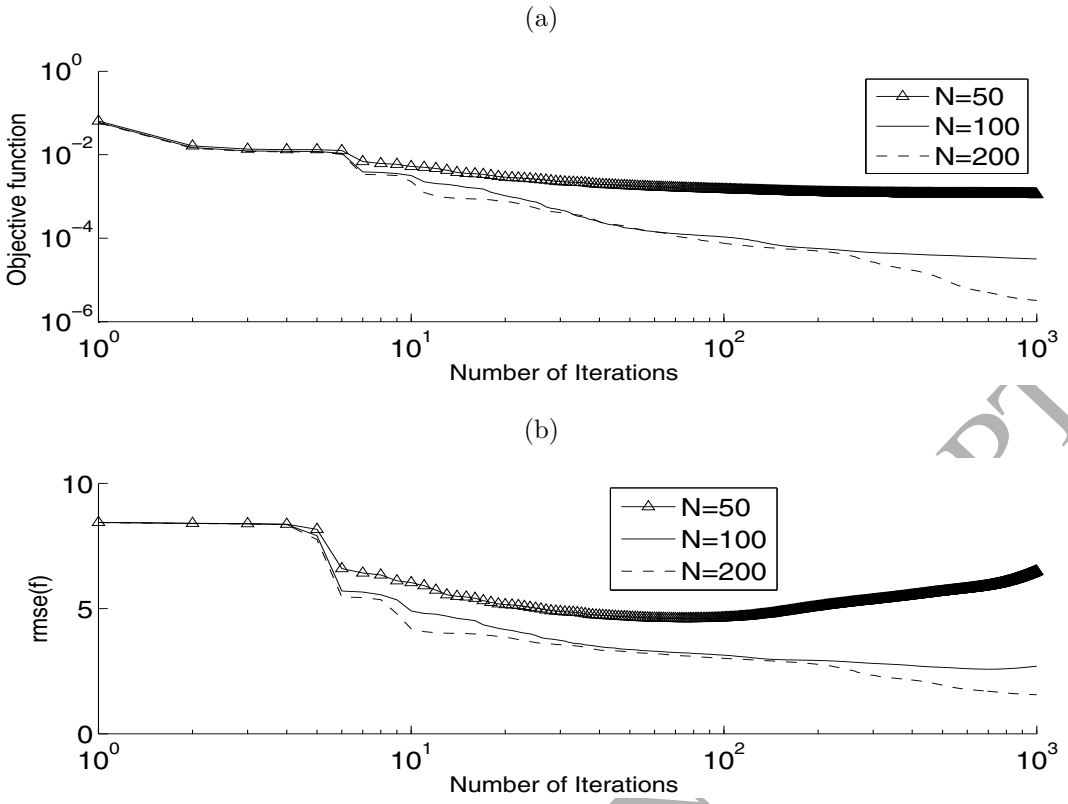

Figure 8: (a) The objective function J_{DN} in (16) and (b) the $rmse(f)$ in (39), as functions of the number of iterations, for $N \in \{50, 100, 200\}$, using the CGM for exact data.

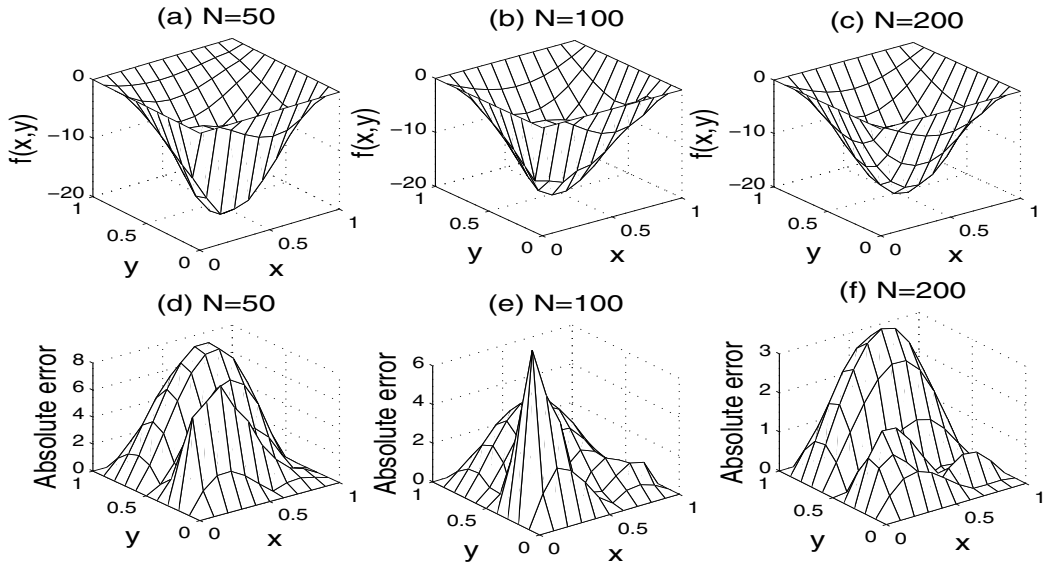

Figure 9: The numerical solutions and the absolute error between the numerical and exact solutions, for the heat source with $N = 50$, plotted at iteration 78 which is the minimum point of $rmse(f)$ in Figure 8(b), $N = 100$, plotted at iteration 715 which is the minimum point of $rmse(f)$ in Figure 8(b), and $N = 200$, using the CGM for exact data.

Next we fix $N = 100$ and consider the case of noisy data (47). Figures 10(a) and 10(b)

show the objective function (16) and the $rmse(f)$, respectively, for the first 10^3 iterations for various percentages of noise $p \in \{5, 10\}\%$ for $\tau = 1.3$. This yields the thresholds in (50) given by $\tau\frac{\epsilon^2(p)}{2} \in \{0.0123, 0.0491\}$ for $p \in \{5, 10\}\%$, respectively. According to the discrepancy principle criterion (50) we cease the CGM iterations at iteration number

$$k_d = \begin{cases} 58, & \text{for } p = 5\%, \\ 37, & \text{for } p = 10\%, \end{cases} \qquad rmse(f_{k_d}) = \begin{cases} 3.5886, & \text{for } p = 5\%, \\ 4.6043, & \text{for } p = 10\%. \end{cases} \tag{59}$$

Also,

$$k_{opt} = \begin{cases} 183, & \text{for } p = 5\%, \\ 224, & \text{for } p = 10\%, \end{cases} \qquad rmse(f_{k_{opt}}) = \begin{cases} 3.0020, & \text{for } p = 5\%, \\ 3.1774, & \text{for } p = 10\%. \end{cases} \tag{60}$$

(a)

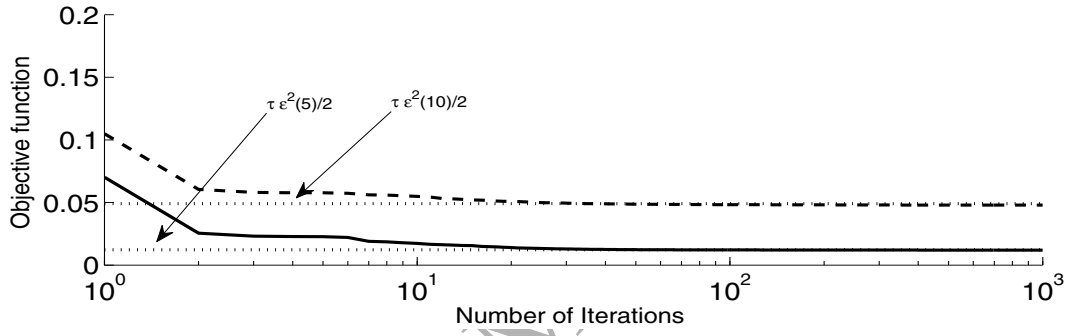

(b)

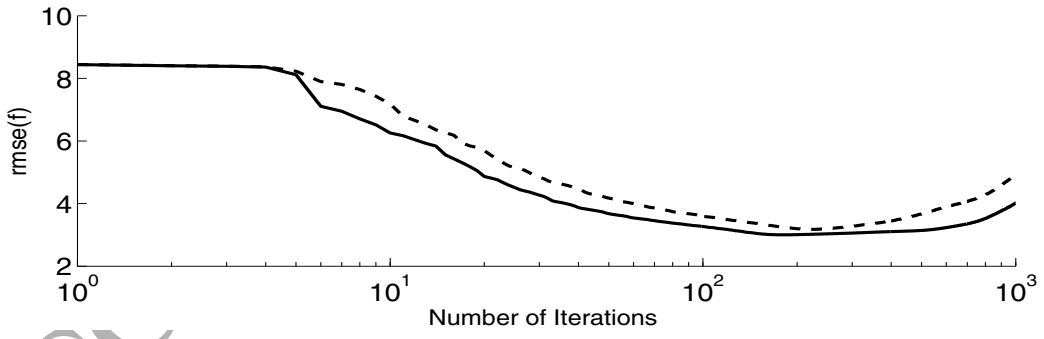

Figure 10: (a) The objective function (16) and (b) the $rmse(f)$, as functions of the number of iterations, using the CGM for various noise levels $p = 5\%$ (—), and $p = 10\%$ (- - -).

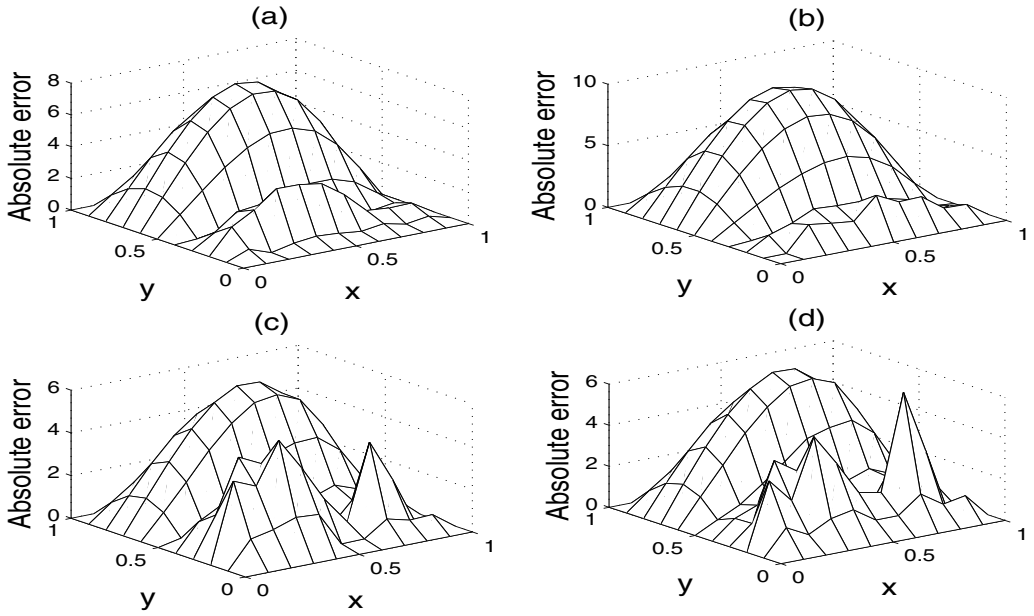

Figure 11: The absolute error between the exact (44) and numerical solutions $f(k_d)$ for (a) $p = 5\%$ and (b) $p = 10\%$ noise. The absolute error between the exact (44) and numerical solutions $f(k_{opt})$ for (c) $p = 5\%$ and (d) $p = 10\%$ noise, using the CGM.

Figure 11 illustrate the numerical solutions for the heat source at the iterations k_d and k_{opt} given by (59) and (60), respectively, for $p \in \{5, 10\}\%$ noise in comparison with exact solution (44). Comparing the expressions (51), (52) and Figure 7 obtained using Landweber method with the expressions (59), (60) and Figure 11 and obtained using CGM it can be seen that the same levels of accuracy and stability are achieved by both iterative regularization methods but the CGM is much faster.

6 Another test example mimicking a point source

In the previous sections 4.2 and 5 we have applied the Landweber method and the CGM, respectively, for solving the inverse problem (2)–(4) and (30) with the input data (41a)–(41c) and (42) having the analytical solution (43) for the temperature and (44) for the heat source.

In this example, we consider reconstructing the function

$$f(x,y) = \frac{1}{a^2\pi} \exp\left(-\frac{(x-x^0)^2 + (y-y^0)^2}{a^2}\right), \tag{61}$$

where $(x^0, y^0) = (0.5, 0.5)$ and $a = 0.3$, mimicking a point source of unit strength/intensity located in the middle of the square plate $\Omega = (0,1)\times(0,1)$. We also take $T = 1$, $r(t) = t+1$ and the data (2) and (3) given by $\phi = 0$ and $\beta = 0$, respectively. As for this data there is no analytical solution available for the temperature u satisfying the Dirichlet direct problem (2), (3) and (30) with f given by (61), the heat flux (4) on $\Gamma = \{0\} \times (0,1)$ is obtained numerically using the FDM. The numerical results obtained for $M_x = M_y = 10$ and various $N \in \{50, 100, 200\}$ are shown in Figures 12(a)–(c), respectively.

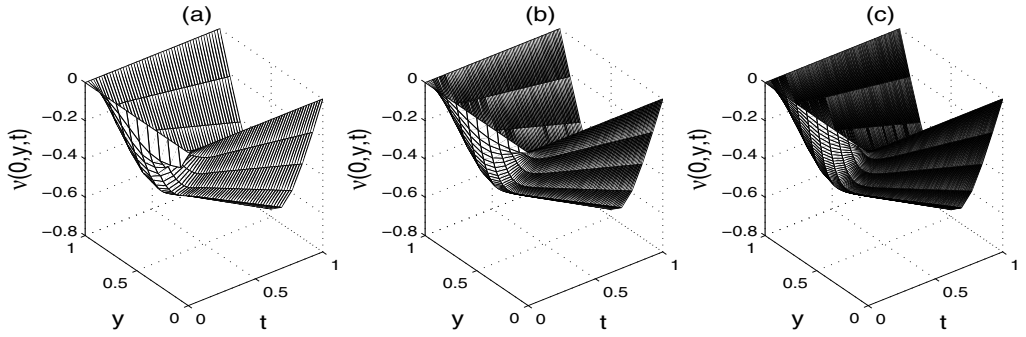

Figure 12: The numerical results for the heat flux $\nu(0, y, t) = \partial_n u(0, y, t)$ obtained by solving the direct problem with $M_x = M_y = 10$ and (a) $N = 50$, (b) $N = 100$ and (c) $N = 200$.

From Figure 12 it can be seen that the numerical solution for the heat flux $\nu(0, y, t)$ is convergent as the time step decreases. Therefore, we consider the numerically simulated flux from Figure 12(c) at every two time steps as the input data (4) for the inverse problem (2)–(4) and (30) which is solved with the $M_x = M_y = 10$ and $N = 100$. This way we avoid committing an inverse crime when numerically simulating the otherwise unavailable input data for the inverse problem. Furthermore, we add $p = 1\%$ noise as in (47), where, from (46) and Figure 12, $\sigma = 0.76\, p$. We take the initial guess $f^0 = 0$.

We apply both the Landweber method (with $\gamma = 5$) and the CGM with $\tau = 1.1$ in the criterion (50) giving the stopping iterations

$$k_d = \begin{cases} 628, & \text{for Landweber,} \\ 164, & \text{for CGM,} \end{cases} \qquad rmse(f_{k_d}) = \begin{cases} 0.4889, & \text{for Landweber,} \\ 0.4946, & \text{for CGM.} \end{cases} \tag{62}$$

Also,

$$k_{opt} = \begin{cases} 6886, & \text{for Landweber,} \\ 1317, & \text{for CGM,} \end{cases} \qquad rmse(f_{k_{opt}}) = \begin{cases} 0.3987, & \text{for Landweber,} \\ 0.3849, & \text{for CGM.} \end{cases} \tag{63}$$

The objective function (45) and the $rmse(f)$ error (39), as functions of the number of iterations, are plotted in Figures 13 (a), (b) and 14 (a), (b), and the corresponding numerical results obtained after k_{opt} and k_d iterations are compared with the analytical solution (61) in Figures 13 (c), (d) and 14 (c), (d), for the Landweber and CGM, respectively. By comparing these figures it can be seen that the CGM is more efficient as it produces faster numerical reconstructions than the Landweber method with the same accuracy, see also equations (62) and (63). In the meantime, both the Landweber and CGM yield stable solutions, as expected, because of their regularizing character and the employment of the discrepancy stopping criterion (50). Although the error between the numerical and exact solutions may seem slightly large, there is noise generated both randomly with $p = 1\%$ as in (46)–(48), as well as numerically as explained above from Figure 12. Furthermore, the inverse problem with $\Gamma = \{0\} \times (0, 1)$ contains limited additional information (yet sufficient for uniqueness but little for stability/accuracy of the reconstruction) on only one side of the unit square and one expects better numerical results if Γ would be increased to contain more sides.

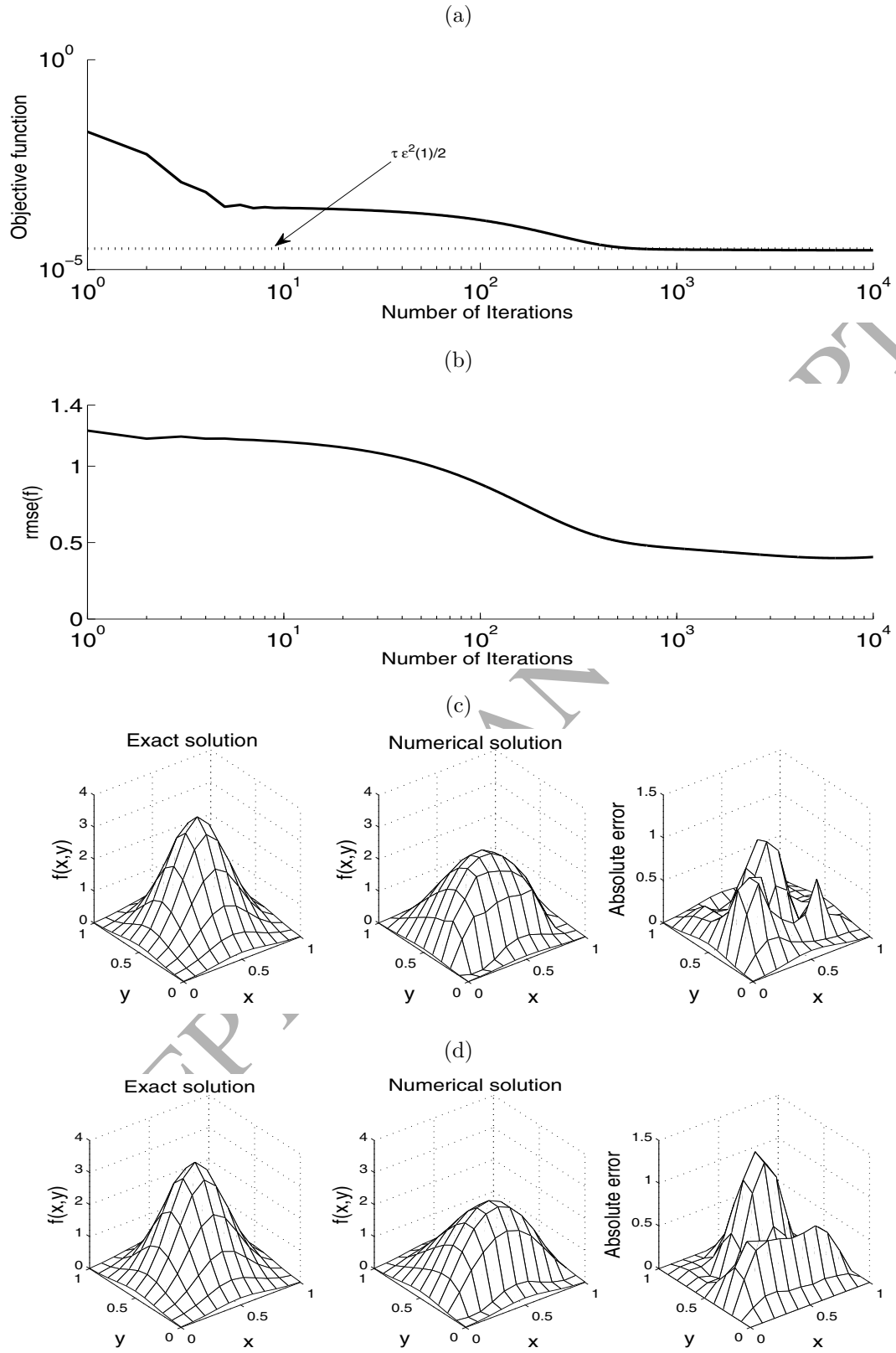

Figure 13: (a) The objective function, (b) the $rmse$, as functions of the number of iterations, the exact (left), numerical (middle) and the absolute error (right) (c) at the iteration $k_{opt} = 6886$ which is the minimum point of $rmse(f)$ and (d) at the iteration $k_d = 628$, for $p = 1\%$ noise, using the Landweber method.

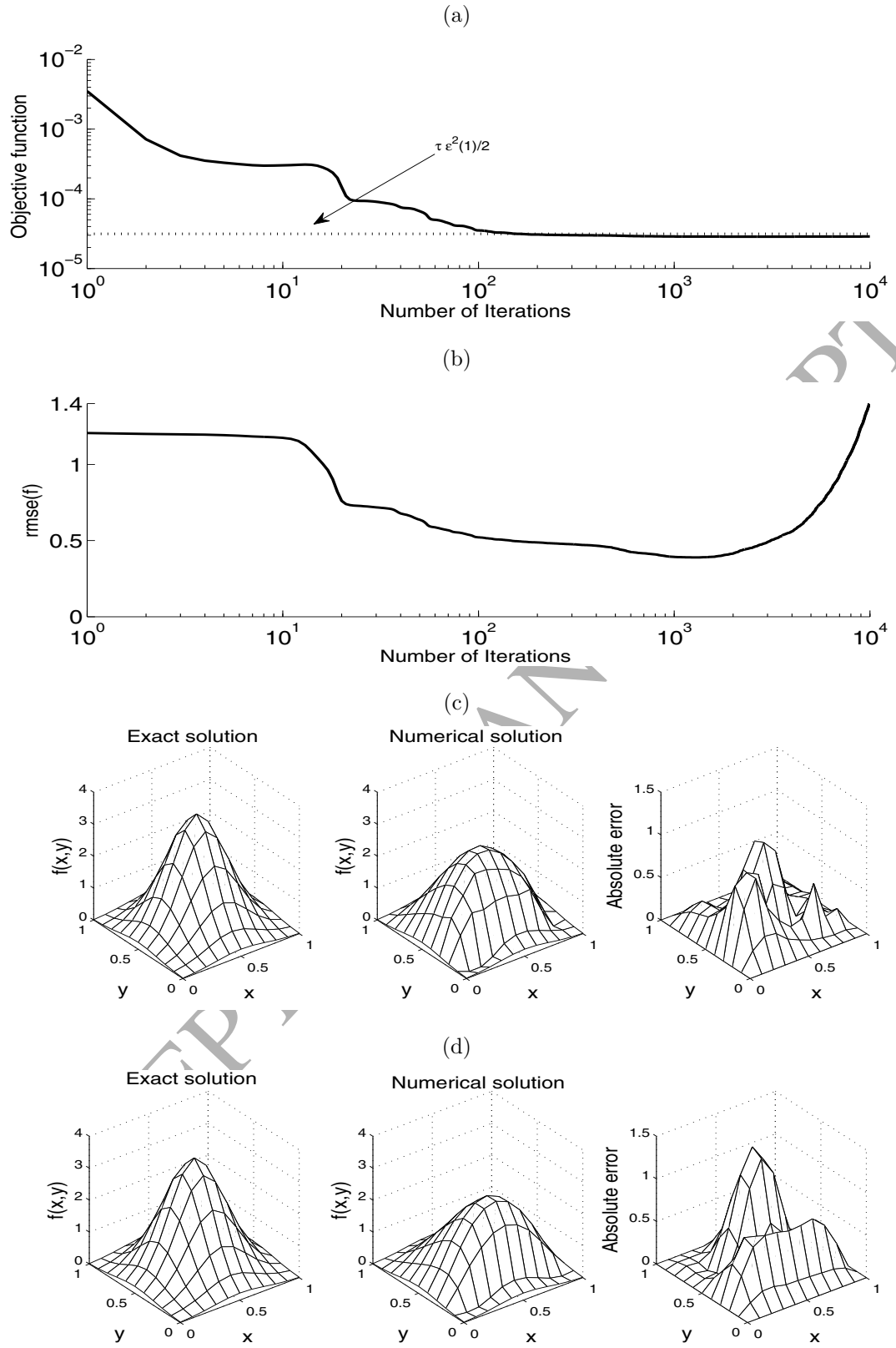

Figure 14: (a) The objective function, (b) the $rmse$, as functions of the number of iterations, the exact (left), numerical (middle) and the absolute error (right) (c) at the iteration $k_{opt} = 1317$ which is the minimum point of $rmse(f)$ and (d) at the iteration $k_d = 164$, for $p = 1\%$ noise, using the CGM.

7 Conclusions

We have presented a computational analysis of the Landweber iterative regularization method for solving the multi-dimensional (with numerical emphasis on the two-dimensional case) inverse heat space-dependent source problem for the heat equation, with Cauchy overprescribed boundary conditions. The Cauchy data is partial in the sense that it is specified only on a small potion Γ of $\partial\Omega$. Thus, the amount of sufficient information to provide the uniqueness of solution is rather minimal and this may be applicable in practical situations concerning limited remote sensing. The CGM has also been developed in order to speed-up the convergence. The direct solver based on ADE finite difference scheme has been employed. Numerical results obtained for both exact and noisy input data show that accurate and stable numerical reconstructions have been achieved. The same conclusions can be obtained for other non-smooth or discontinuous source examples, as shown elsewhere for related inverse source problems, [2, 5, 6].

Future work will consist in extending the analysis and methods of this study to the simultaneous reconstruction of multi-dimensional space-dependent source and diffusivity coefficient, [20].

References

[1] M.N. Ahmadabadi, M. Arab, F. Maalek-Ghaini, The method of fundamental solutions for the inverse space-dependent heat source problem, Eng. Anal. Boundary Elements 33 (2009) 1231–1235.

[2] A. Erdem, D. Lesnic, A. Hasanov, Identification of a spacewise dependent heat source, Appl. Math. Model. 37 (2013) 10231–10244.

[3] A. Farcas, D. Lesnic, The boundary-element method for the determination of a heat source dependent on one variable, J. Eng. Math. 54 (2006) 375–388.

[4] A. Hasanov, B. Pektaş, A unified approach to identifying an unknown spacewise dependent source in a variable coefficient parabolic equation from final and integral overdeterminations, Appl. Numer. Math. 78 (2014) 49–67.

[5] B.T. Johansson, D. Lesnic, A variational method for identifying a spacewise-dependent heat source, IMA J. Appl. Math. 72 (2007) 748–760.

[6] B.T. Johansson, D. Lesnic, Determination of a spacewise dependent heat source, J. Comput. Appl. Math. 209 (2007) 66–80.

[7] D.D. Trong, P.H. Quan, P.N. Dinh Alain, Determination of a two-dimensional heat source: Uniqueness, regularization and error estimate, J. Comput. Appl. Math. 191 (2006) 50–67.

[8] W. Wang, M. Yamamoto, B. Han, Two-dimensional parabolic inverse source problem with final overdetermination in reproducing kernel space, Chinese Annals of Mathematics, Series B, 35B (2014) 469–482.

[9] L. Yan, F.L. Yang, C.L. Fu, A meshless method for solving an inverse spacewise-dependent heat source problem, J. Comput. Phys. 228 (2009) 123–136.

[10] J.R. Cannon, Determination of an unknown heat source from overspecified boundary data, SIAM J. Numer. Anal. 5 (1968) 275–286.

[11] M. Yamamoto, Conditional stability in determination of force terms of heat equations in a rectangle, Math. Comput. Model. 18 (1993) 79–88.

[12] Dinh Nho Hao, Methods for Inverse Heat Conduction Problems, Peter Lang, Frankfurt am Main, 1998.

[13] H.W. Engl, O. Scherzer, M. Yamamoto, Uniqueness and stable determination of forcing terms in linear partial differential equations with overspecified boundary data, Inverse Problems 10 (1994) 1253-1276.

[14] O.A. Ladyzenskaja, V.A. Solonnikov, N.N. Uralceva, Linear and Quasi-linear Equations of Parabolic Type, American Mathematical Society, Providence, 1968.

[15] A. Pazy, Semigroups of Linear Operators and Applications to Partial Differential Equations, Springer Science & Business Media, New York, 2012.

[16] H.W. Engl, M. Hanke, A. Neubauer, Regularization of Inverse Problems, Kluwer Academic, Dordrecht, 1996.

[17] A. Hasanov, An inverse source problem with single Dirichlet type measured output data for a linear parabolic equation, Appl. Math. Lett. 24 (2011) 1269–1273.

[18] A. Hasanov, M. Otelbaev, B. Akpayev, Inverse heat conduction problems with boundary and final time measured output data, Inverse Problems Sci. Eng. 19 (2011) 985–1006.

[19] H.Z. Barakat, J.A. Clark, On the solution of the diffusion equations by numerical methods, J. Heat Transfer, 88 (1966) 421–427.

[20] C. Coles, D.A. Murio, Simultaneous space diffusivity and source term reconstruction in 2D IHCP, Comput. Math. Appl. 42 (2001) 1549–1564.